CLNS 95/1354
CLEO 95-16

CALTECH UC - SAN DIEGO UC - SANTA BARBARA CARLETON COLORADO
CORNELL FLORIDA HARVARD ILLINOIS ITHACA KANSAS MCGILL
MINNESOTA OHIO STATE OKLAHOMA PURDUE ROCHESTER
SOUTHERN - METHODIST SYRACUSE SUNY - ALBANY VANDERBILT VIRGINIA TECH

Measurements of $B \to D_s^+ X$ Decays

CLNS 95/1354

CLEO 95-16

Measurements of $B \to D_s^+ X$ Decays

D. Gibaut, K. Kinoshita, and P. Pomianowski

Virginia Polytechnic Institute and State University, Blacksburg, Virginia, 24061

B. Barish, M. Chadha, S. Chan, D.F. Cowen, G. Eigen, J.S. Miller, C. O'Grady, J. Urheim, A.J. Weinstein, and F. Würthwein

California Institute of Technology, Pasadena, California 91125

D.M. Asner, M. Athanas, D.W. Bliss, W.S. Brower, G. Masek, and H.P. Paar

University of California, San Diego, La Jolla, California 92093

J. Gronberg, C.M. Korte, R. Kutschke, S. Menary, R.J. Morrison, S. Nakanishi, H.N. Nelson, T.K. Nelson, C. Qiao, J.D. Richman, D. Roberts, A. Ryd, H. Tajima, and M.S. Witherell

University of California, Santa Barbara, California 93106

R. Balest, K. Cho, W.T. Ford, M. Lohner, H. Park, P. Rankin, and J.G. Smith

University of Colorado, Boulder, Colorado 80309-0390

J.P. Alexander, C. Bebek, B.E. Berger, K. Berkelman, K. Bloom, T.E. Browder,* D.G. Cassel, H.A. Cho, D.M. Coffman, D.S. Crowcroft, M. Dickson, P.S. Drell, D.J. Dumas, R. Ehrlich, R. Elia, P. Gaidarev, M. Garcia-Sciveres, B. Gittelman, S.W. Gray, D.L. Hartill, B.K. Heltsley, S. Henderson, C.D. Jones, S.L. Jones, J. Kandaswamy, N. Katayama, P.C. Kim, D.L. Kreinick, T. Lee, Y. Liu, G.S. Ludwig, J. Masui, J. Mevissen, N.B. Mistry, C.R. Ng, E. Nordberg, J.R. Patterson, D. Peterson,

D. Riley, and A. Soffer

Cornell University, Ithaca, New York 14853

P. Avery, A. Freyberger, K. Lingel, J. Rodriguez, S. Yang, and J. Yelton

University of Florida, Gainesville, Florida 32611

G. Brandenburg, D. Cinabro, T. Liu, M. Saulnier, R. Wilson, and H. Yamamoto

Harvard University, Cambridge, Massachusetts 02138

T. Bergfeld, B.I. Eisenstein, J. Ernst, G.E. Gladding, G.D. Gollin, M. Palmer, M. Selen, and J.J. Thaler

University of Illinois, Champaign-Urbana, Illinois, 61801

K.W. Edwards, K.W. McLean, and M. Ogg

Carleton University, Ottawa, Ontario K1S 5B6 and the Institute of Particle Physics, Canada

A. Bellerive, D.I. Britton, E.R.F. Hyatt, R. Janicek, D.B. MacFarlane, P.M. Patel, and B. Spaan

McGill University, Montréal, Québec H3A 2T8 and the Institute of Particle Physics, Canada

A.J. Sadoff

Ithaca College, Ithaca, New York 14850

R. Ammar, P. Baringer, A. Bean, D. Besson, D. Coppage, N. Copty, R. Davis, N. Hancock, M. Kelly, S. Kotov, I. Kravchenko, N. Kwak, and H. Lam

University of Kansas, Lawrence, Kansas 66045

Y. Kubota, M. Lattery, M. Momayezi, J.K. Nelson, S. Patton, R. Poling, V. Savinov, S. Schrenk, and R. Wang

University of Minnesota, Minneapolis, Minnesota 55455

M.S. Alam, I.J. Kim, Z. Ling, A.H. Mahmood, J.J. O'Neill, H. Severini, C.R. Sun, and F. Wappler

State University of New York at Albany, Albany, New York 12222

G. Crawford, R. Fulton, D. Fujino, K.K. Gan, K. Honscheid, H. Kagan, R. Kass, J. Lee, M. Sung, C. White, A. Wolf, and M.M. Zoeller

Ohio State University, Columbus, Ohio, 43210

X. Fu, B. Nemati, W.R. Ross, P. Skubic, and M. Wood

University of Oklahoma, Norman, Oklahoma 73019

M. Bishai, J. Fast, E. Gerndt, J.W. Hinson, R.L. McIlwain, T. Miao, D.H. Miller, M. Modesitt, D. Payne, E.I. Shibata, I.P.J. Shipsey, and P.N. Wang

Purdue University, West Lafayette, Indiana 47907

L. Gibbons, Y. Kwon, S. Roberts, and E.H. Thorndike

University of Rochester, Rochester, New York 14627

T.E. Coan, J. Dominick, V. Fadeyev, I. Korolkov, M. Lambrecht, S. Sanghera, V. Shelkov, T. Skwarnicki, R. Stroynowski, I. Volobouev, and G. Wei

Southern Methodist University, Dallas, Texas 75275

M. Artuso, M. Gao, M. Goldberg, D. He, N. Horwitz, G.C. Moneti, R. Mountain, F. Muheim, Y. Mukhin, S. Playfer, Y. Rozen, S. Stone, X. Xing, and G. Zhu

Syracuse University, Syracuse, New York 13244

J. Bartelt, S.E. Csorna, Z. Egyed, and V. Jain

Vanderbilt University, Nashville, Tennessee 37235

(CLEO Collaboration)

Abstract

This paper describes new measurements from CLEO of the inclusive $B \to D_s^+ X$ branching fraction as well as the $B^+ \to D_s^{(*)+} \bar{D}^{(*)0}$ and $B^0 \to D_s^{(*)+} D^{(*)-}$ branching fractions. The inclusive branching fraction is $\mathcal{B}(B \to D_s^+ X) = (12.11 \pm 0.39 \pm 0.88 \pm 1.38)\%$ where the first error is statistical, the second is the systematic error, and the third is the error due to the uncertainty in the $D_s^+ \to \phi\pi^+$ branching fraction. The branching fractions for the $B \to D_s^{(*)+} \bar{D}^{(*)}$ modes are found to be between 0.9% and 2.4% and are significantly more precise than previous measurements. The sum of the $B \to D_s^{(*)+} \bar{D}^{(*)}$ branching fractions is consistent with the results of fits to the inclusive D_s^+ momentum spectrum. Factorization is used to arrive at a value for f_{D_s}, the D_s^+ decay constant.

13.25.Hw

Typeset using REVTEX

*Permanent address: University of Hawaii at Manoa

I. INTRODUCTION

The large samples of B mesons being collected by experimental groups at e^+e^- and hadron colliders have allowed for ever more precise measurements of B meson decay properties. Theoretical calculations are unable to simultaneously describe the total inclusive B to charm rate and the semi-leptonic branching fraction of the B meson [1]. It has been conjectured that b quark to charm quark transitions where the W^+ materializes as $\bar{c}s$ are large [2]. The external spectator B meson decay diagram, shown in Figure 1, leads to a $D_s^{(*)+}$ in the final state whereas the internal W^+ decay diagram results in the production of charmonium [3]. This paper reports new measurements of $B \to D_s^+ X$ decays from CLEO[1].

After a short description of the detector and the criteria used to select neutral and charged particle candidates, there are two sections dealing with the measurements of the inclusive $B \to D_s^+ X$ branching fraction and the exclusive $B \to D_s^{(*)+} \bar{D}^{(*)}$ branching fractions. Under the assumption that the charged and neutral B decay rates and lifetimes are equal, the charged and neutral B branching fractions are averaged and compared with theoretical predictions. This is followed by a discussion of a fit to the inclusive D_s^+ momentum spectrum. The final section describes two methods using factorization to extract f_{D_s}, the D_s^+ decay constant.

---

[1]Reference to a specific state or decay means that the charge-conjugate state or decay has been included. The notation $D_s^{+(*)}$ in this context means either D_s^+ or D_s^{*+}. In $B \to D_s^{(*)+} \bar{D}^{(*)}$, $\bar{D}$ is a generic representation of the $\bar{c}q$ mesons, the D^- and $\bar{D}^0$, while the symbol $(*)$ implies that the branching fraction for both the nonexcited and excited states of the meson were separately measured.

II. EVENT AND TRACK SELECTION

The data used in this analysis were selected from hadronic events produced in e^+e^- annihilations at the Cornell Electron Storage Ring (CESR). The data sample consists of an integrated luminosity of 2.03 ± 0.04 fb^{-1} collected at the $\Upsilon(4S)$ resonance (refered to as on-resonance data) and 0.97 ± 0.02 fb^{-1} at a center-of-mass energy just below the threshold for producing $B\bar{B}$ mesons (refered to as off-resonance or continuum data). The on-resonance data corresponds to $(2.19 \pm 0.04) \times 10^6$ $B\bar{B}$ pairs.

The CLEO II detector measures both neutral and charged particles with excellent resolution and efficiency [4]. Hadronic events are selected by requiring a minimum of three charged tracks, a total visible energy greater than 15% of the center-of-mass energy (this reduces contamination from two-photon interactions and beam-gas events), and a primary vertex within ± 5 cm in the z-direction and ± 2 cm in the r-ϕ plane of the nominal collision point. Since the B mesons are produced almost at rest, their decay products are uniformly distributed throughout the volume of the detector leading to events that tend to be "spherical" in shape. Continuum $e^+e^- \rightarrow q\bar{q}$ ($q = u, d, s, c$) events are more jet-like in structure. The shape variable R_2, which is is the ratio of the second Fox-Wolfram moment to the zeroth moment [5], is found to be useful in discriminating between $B\bar{B}$ events and those in which lighter mass quarks are produced. Only events with $R_2 < 0.35$ are used in this analysis.

All charged tracks are required to be consistent with having originated from within ± 5 cm in the z-direction and ± 5 mm in the r-ϕ plane of the primary vertex. Tracks are also required to have dE/dx information which is consistent with the proposed particle hypothesis.

III. THE INCLUSIVE $B \rightarrow D_S^+ X$ BRANCHING FRACTION

The D_s^+ mesons in the on-resonance data set originate from B meson decays and from continuum production via $e^+e^- \rightarrow c\bar{c}$. Therefore, in order to measure $\mathcal{B}(B \rightarrow D_s^+ X)$, it is necessary to subtract the continuum contribution from the total yield of D_s^+ mesons in the

on-resonance data set.

The $D_s^+ \to \phi\pi^+$, $\phi \to K^+K^-$ decay channel was chosen for the inclusive $B \to D_s^+ X$ measurement because it offers the best combination of detection efficiency, branching fraction, and signal to background ratio. The K^+K^- invariant mass is required to be within 10 MeV of the ϕ mass. Two angles are useful for suppressing background: 1) the ϕ helicity angle, θ_H, which is the angle in the ϕ rest frame between the direction of the K^+ and the D_s^+ direction, and 2) the D_s^+ decay angle, θ_D, which is the angle in the D_s^+ rest frame between the ϕ direction and D_s^+ direction in the lab frame. The signal follows a $\cos^2\theta_H$ distribution while the background is flat in $\cos\theta_H$ so requiring $|\cos\theta_H| > 0.35$ eliminates 35% of the background events while retaining 96% of the signal. The $\cos\theta_D$ distribution for the signal is flat. The $\cos\theta_D < 0.75$ requirement suppresses combinatorial background from abundant low momentum pions that peaks near $\cos\theta_D = 1$.

The efficiency of these selection criteria is calculated from a Monte Carlo simulation. Figure 2 shows the D_s^+ detection efficiency as a function of x, the scaled D_s^+ momentum, where $x \equiv p_{D_s^+}/p_{max}$ and $p_{max} = \sqrt{E_{beam}^2 - m_{D_s^+}^2}$. The endpoint for D_s^+ mesons produced in B decay is $x = 0.46$.

The on-resonance yield of D_s^+ mesons as a function of scaled momentum is extracted by fitting the $\phi\pi^+$ invariant mass plot in bins of x. The bin size of 0.03 is an order of magnitude larger than the resolution in x. The fitting function consists of a straight line parameterization of the combinatorial background and a Gaussian describing the signal. The width of the Gaussian is fixed to the value found from fitting the Monte Carlo sample. The r.m.s. resolution increases linearly with momentum from 6 MeV at low momentum to 8 MeV as x approaches 1. The D_s^+ mass was allowed to vary as a function of momentum in a first pass of fitting to the data and then was fixed to the average value of 1.9686 GeV in the final pass. For illustration purposes, the $\phi\pi^+$ mass spectra and resultant fits for an x bin width of 0.07 are shown in Figure 3. The D_s^+ momentum spectrum before efficiency correction is shown in Figure 4.

The fact that there are no D_s^+ mesons from B decay with $x > 0.5$ is used to create a continuum momentum spectrum with maximum statistics. The momentum spectrum for continuum produced D_s^+ mesons is constructed from the sum of the on- and off-resonance data for $x > 0.5$ and only the off-resonance data, scaled by the ratio of on/off luminosities, for $x < 0.5$. The number of D_s^+ mesons per momentum bin for this "constructed" continuum data sample is extracted in the same manner as described above. The resulting continuum D_s^+ momentum spectrum, properly rescaled, is shown in Figure 4. It is fit with a function that was found to describe the Monte Carlo continuum D_s^+ momentum spectrum. The values of this function, also shown in Figure 4, are subtracted, bin by bin, from the on-resonance D_s^+ momentum spectrum to give the raw (i.e., not efficiency corrected) yield of 2537 ± 83 D_s^+ mesons produced in B decays.

Figure 5 shows the D_s^+ momentum spectrum after continuum subtraction and correction for detection efficiency. From the total yield of 9111 ± 299 D_s^+ mesons from B decay, the inclusive branching fraction is calculated to be:

$$\mathcal{B}(B \to D_s^+ X) = \left[(12.11 \pm 0.39 \pm 0.88) \times \left(\frac{3.5 \pm 0.4\%}{\mathcal{B}(D_s^+ \to \phi\pi^+)} \right) \right] \%$$

where the first error is statistical, the second is the systematic error, and the third error is due to the uncertainty in the $D_s^+ \to \phi\pi^+$ branching fraction [6]. This value for $\mathcal{B}(B \to D_s^+ X)$ is larger than the previous CLEO and ARGUS measurements shown in Table I.

The largest error in the measurement is the 11% uncertainty in the $D_s^+ \to \phi\pi^+$ branching fraction. This error is displayed separately to distinguish it from the 7.2% systematic error associated with detector effects and the analysis method. The contributions to the systematic error are listed in Table II. The uncertainties in the number of $B\bar{B}$ pairs and in the $\phi \to K^+K^-$ branching fraction are included but the dominant source is the uncertainty in the tracking efficiency. A 2% per track uncertainty in the track finding efficiency results in a 6% systematic error for the $D_s^+ \to \phi\pi^+, \phi \to K^+K^-$ decay chain. The other sources of systematic error on the D_s^+ yield listed in Table II contribute 3.1% to the total systematic error.

IV. EXCLUSIVE $B \to D_S^{(*)+} \bar{D}^{(*)}$ DECAYS

The near hermeticity of the CLEO II detector coupled with its excellent photon detection and charged particle reconstruction capabilities allow for the reconstruction of all eight $B^0 \to D_s^{(*)+} D^{(*)-}$ and $B^+ \to D_s^{(*)+} \bar{D}^{(*)0}$ modes. The $D_s^{(*)+}$ and $D^{(*)}$ decay channels used, the mass selection criteria, and the assumed branching fractions, are given in Tables III and IV. The allowed mass intervals correspond to 2.5 standard deviations for channels where the mass resolution dominates the observed width, and to one natural width otherwise. The D_s^+ and D^0 branching fractions are given relative to those for the two normalizing modes; $D_s^+ \to \phi\pi^+$ and $D^0 \to K^-\pi^+$. The values for all absolute branching fractions and relative branching ratios are taken from [6] except for $\mathcal{B}(D^0 \to K^-\pi^+)$ [11], $\mathcal{B}(D^+ \to K^-\pi^+\pi^+)/\mathcal{B}(D^0 \to K^-\pi^+)$ [12], and the D^* branching fractions [13], where CLEO measurements are used since they dominate the world average and their use allows for the cancellation of some common systematic errors.

The data sample and the event selection criteria are the same as were used in the inclusive analysis. The track quality criteria are also the same except for the "slow" π^+ from $D^{*+} \to D^0\pi^+$ decays which has just the r-ϕ distance of closest approach requirement applied. Photon candidates are required to have deposited more than 30 MeV of energy in the calorimeter, to be isolated from charged tracks, and to have a lateral energy deposition consistent with that expected for a photon. Photons used for reconstructing the $D_s^{*+} \to D_s^+\gamma$ decay chain have a minimum energy requirement of 90 MeV and must have been detected within the "barrel" region of the detector, defined by $|\cos\theta| < 0.707$ where θ is the angle between the photon momentum vector and the z axis. For π^0 or η mesons, one of the daughter photons can be from outside of barrel where the minimum photon energy requirement is raised to 50 MeV.

The allowed mass intervals and branching fractions for the various non-charmed resonances used in this analysis are given in Table V. In π^0/η decays to two photons, the decay angle, θ_D, which is the angle in the π^0/η rest frame between the direction of one the photons and the π^0/η direction in the lab frame, can be used to reduce combinatorial background

from low energy photons. A $|\cos\theta_D| < 0.9$ criterion is used.

Since the $\Upsilon(4S)$ decays only to $B\bar{B}$, the B meson energy is equal to the beam energy. This can be used to select B meson candidates by requiring that ΔE, the difference between the measured sum of the charged and neutral energies of the daughters of the B candidate and the beam energy, be close to zero. The $D_s^{(*)+}$ and $D^{(*)}$ candidates, as well as the π^0 and η candidates, are kinematically fitted to their known masses so as to improve the resolution in ΔE. The ΔE resolution is about 10 MeV and is independent of decay mode according to a Monte Carlo simulation of $B \to D_s^{(*)+}\bar{D}^{(*)}$ events[2]. All B candidates must have $|\Delta E| \leq 25$ MeV. In the case of multiple candidates in a specific B meson decay chain, only the candidate with the smallest absolute value of ΔE is selected. The B mass resolution can be improved by using the beam-constrained mass (M_B), defined by:

$$M_B^2 = E_{beam}^2 - \left(\sum_i \vec{p}_i\right)^2, \tag{1}$$

where $\vec{p}_i$ is the momentum of the i-th daughter of the B candidate. The M_B resolution of about 2.6 MeV is determined by the beam energy spread and is a factor of ten better than the resolution in invariant mass obtained from simply summing the 4-momenta of the B daughters.

Two other useful variables are the B production angle, θ_B, which is the angle between the B meson direction in the lab frame and the beam axis, and the sphericity angle, θ_S, which is the angle between the sphericity axis of the particles which form the B candidate and the sphericity axis of the other particles in the event. For B mesons, the production angle follows a $\sin^2\theta_B$ distribution whereas the continuum background is flat in this variable. Conversely, continuum events have large values of $\cos\theta_S$ whereas the signal is flat in $\cos\theta_S$. The production and sphericity angle criteria are B decay channel dependent because of differing background levels. A helicity angle requirement is also used for the $D_s^+\bar{D}^*$ final

---

[2]This occurs because the low momentum π^+, π^0, or γ that differentiates the eight different modes contributes negligibly to the ΔE resolution.

states where the signal follows a $\cos^2\theta_H$ distribution, and for the $D_s^{*+}\bar{D}$ final states where the signal follows a $\sin^2\theta_H$ distribution. The values of the angular selection criteria used in the analysis are given in Table VI.

The beam-constrained mass plot for the sum of the eight B^0 and B^+ decay channels is shown in Figure 6. The function which is fitted to the data to extract the yield of B mesons contains two parts: 1) a background function which is linear for $M_B < 5.282$ GeV and parabolic, with a kinematic cutoff, for larger values of M_B [14], and 2) a Gaussian to describe the signal. The background function is forced to simultaneously fit the beam-constrained mass distribution for the ΔE sideband, defined by $30 < |\Delta E| < 55$ MeV, so as to better constrain the shape of the background. This is essential for some of the decay channels where the number of background events is insufficient to constrain the background. The mass and width from the fit to the sum of all modes are consistent with those obtained from the Monte Carlo. The total in the peak is 171 ± 18 events.

The beam-constrained mass plots for the individual B^0 and B^+ decay channels are shown in Figures 7 and 8. The mass and width for these fits are fixed to the value obtained from the fit to the sum of all the modes.

The branching fractions are calculated as follows[3]:

$$\mathcal{B}(B \to D_s^{(*)+}\bar{D}^{(*)}) = \frac{1}{N_{B\overline{B}}} \frac{N_{D_s^{(*)+}\bar{D}^{(*)}}}{\sum_i \sum_j \mathcal{B}_i \mathcal{B}_j \varepsilon_{ij}}, \tag{2}$$

where $N_{B\overline{B}}$ is the number of $B\bar{B}$ pairs, $N_{D_s^{(*)+}\bar{D}^{(*)}}$ is the number of signal events extracted from the fit to the beam-constrained mass distribution, $\mathcal{B}_i$ is the branching fraction of the i^{th} charm decay mode, and ε_{ij} is the reconstruction efficiency for the combination of the i^{th} D_s^+ decay channel and the j^{th} $\bar{D}$ decay channel [15]. The resulting exclusive branching fractions are listed in Table VII where the first error is the statistical error, the second error is the systematic error from all sources other than the uncertainty in the normalizing branching fractions, $\mathcal{B}(D_s^+ \to \phi\pi^+)$ and $\mathcal{B}(D^0 \to K^-\pi^+)$, and the third error is that due to

---

[3]Equal production of charged and neutral B mesons is assumed.

the uncertainty in the normalizing branching fractions, which is completely dominated by the uncertainty in $\mathcal{B}(D_s^+ \to \phi\pi^+)$.

The systematic errors associated with the uncertainty in the detection efficiencies of charged tracks and neutral clusters are calculated in the following manner. A tracking efficiency error of 2% per track is assumed except for the "slow" π^+ from $D^{*+} \to D^0\pi^+$ decays where an additional 4.6% is added in quadrature (making the total systematic error for the slow pion to be 5%). This additional error arises because the tracking efficiency is rising sharply at low momentum. The tracking errors add linearly except for the additional 4.6% on the slow pion. For example, for the $D^{*+} \to D^0\pi^+$, $D^0 \to K^-\pi^+\pi^+\pi^-$ decay chain, the systematic error associated with tracking is $\sqrt{(5 \times 2)^2 + 4.6^2} = 11\%$. The systematic errors associated with neutrals, 3% per photon and 5% per π^0 or η, are also added linearly. The charged and neutral systematic errors are then added in quadrature. The total systematic error due to uncertainties in efficiencies is then the weighted average of the systematic errors of the particular decay channels where the weight is $\varepsilon \cdot \mathcal{B}$ for that particular decay channel. The systematic error due to the uncertainties in the relative branching fractions is calculated in the same manner. These are the two dominant sources of systematic error.

The other possible sources of systematic error which were investigated include: cross-feed between the eight channels, uncertainty in the efficiency due to the method of choosing the candidate with the smallest $|\Delta E|$, parameterization of the background in the beam-constrained mass plots, and particle identification requirements. There is a non-negligible contribution to the systematic error due to the background parameterization for the $B \to D_s^+\bar{D}$ modes where the background in the beam-constrained mass plot is significant.

V. THE $B \to D_S^{(*)+}\bar{D}^{(*)}$ DECAY RATES

In the dominant process leading to a two-body decay of the type $B \to D_s^{(*)+}D^{(*)}$, shown in Figure 1, the $D_s^{(*)+}$ is produced from the fragmentation of the W^+. The analogous $b \to u$ transitions lead to final states like $D_s^+\pi^-$ but these decay rates are down by roughly

$|V_{ub}/V_{cb}|^2 \approx 0.006$ compared to $b \to c$ transitions [16,17]. A D_s^+ is not produced in internal W^+ decay. The decay $B \to D_s^{(*)+}\bar{D}^{(*)}$ can also proceed through the "penguin" decay mode $\bar{b} \to \bar{s}g, g \to c\bar{c}$ but this is expected to be small. Other processes, such as annihilation and W-exchange, lead to final states like $D_s^+ K^{(*)}$ but there is no evidence that these processes are significant in B meson decay [16,17]. None of these scenarios lead to a significant difference in the charged and neutral $B \to D_s^{(*)+}\bar{D}^{(*)}$ decay rates.

The equivalence of the charged and neutral decay rates can be tested using the exclusive branching fractions and $\tau(B^+)/\tau(B^0) \equiv \tau_{+/0} = 0.98 \pm 0.09$ [6]. The results are given in Table VIII where, for a given decay mode (e.g., $B \to D_s^+ \bar{D}^*$), $\mathcal{B}^{+(0)}$ denotes the branching fraction for the charged (neutral) B to decay via this mode. Most of the sytematic errors cancel when calculating $\mathcal{B}^0/\mathcal{B}^+$ except for the 10% uncertainty in $\mathcal{B}(D^+ \to K^-\pi^+\pi^+)/\mathcal{B}(D^0 \to K^-\pi^+)$ [12] and the 7% error in the π^0/π^+ efficiencies [18] which comes in directly when taking the ratios of modes involving D^{*0} and D^{*+} mesons. The mean value of $\Gamma(B^0 \to D_s^{(*)+}D^{(*)-})/\Gamma(B^+ \to D_s^{(*)+}\bar{D}^{(*)0})$ of $0.69 \pm 0.13 \pm 0.11$ is not inconsistent with the decay rates for the charged and neutral B mesons being equal.

Assuming that the charged and neutral decay rates are equal, and that $\tau_{+/0} = 1$, it is reasonable to calculate the average branching fractions. For a particular $B \to D_s^{(*)+}\bar{D}^{(*)}$ decay channel the yield is extracted from a fit to the sum of the $B^0 \to D_s^{(*)+}D^{(*)-}$ and $B^+ \to D_s^{(*)+}\bar{D}^{(*)0}$ beam-constrained mass distributions. The average branching fraction is then calculated as in equation (2). The results are given in Table VIII.

VI. FACTORIZATION AND PREDICTIONS FOR TWO-BODY RATES

Predictions for exclusive branching fractions have been made using the factorization ansatz. This method was pioneered by Bauer, Stech, and Wirbel (BSW) [19]. Any calculation of widths using factorization arrives at an equation of the following form:

$$\mathcal{B}(B \to D_s^{(*)+}\bar{D}^{(*)}) = KG_F^2 a_1^2 |V_{cb}V_{cs}^*|^2 f_{D_s^{(*)}}^2 F_{(*)}^2 \tau_B \qquad (3)$$

where K is a kinematic factor and $F_{(*)}$ is the form factor term (summed over polarizations for decays involving D^* mesons, etc.). The factorization parameter a_1 is the relevant one for external spectator decays. The difference between the predictions comes from the form factor term. BSW use a simple pole form while other calculations [20-24] use form factors motivated by Heavy Quark Effective Theory (HQET) [25]. Several predictions are given in Table IX along with the measured average branching fractions.

While there are significant differences between the predictions for any particular branching fraction, the variations in the predictions for the ratios of the decay widths due to the different parameterizations of the form factors are smaller. These predictions are given in Table X. The decay constant dependence is given explicitly in Table X although, in the heavy quark limit, the vector and pseudoscalar decay constants are equal. More precisely, $f_P^2 = f_V^2 = 12|\Psi(0)|^2/M$ where $|\Psi(0)|$ is the wave function of the light antiquark and heavy quark at zero relative separation, and M is the heavy-meson mass [21]. As can be seen in Table X, taking $f_{D_s^*} = f_{D_s}$, the $B \to D_s^{*+}\bar{D}$ and $B \to D_s^+\bar{D}^*$ widths are predicted to be roughly equal. It was assumed in [19] that $(f_{D_s^*}/f_{D_s})^2 = 1.86$ leading to their prediction that $\Gamma(B \to D_s^{*+}\bar{D})$ is some 2.5 times larger than $\Gamma(B \to D_s^+\bar{D}^*)$.

The experimental results for the ratios of widths are given in the last row of Table X. The quoted error is the sum of the statistical and systematic errors added in quadrature. Most of the experimental systematic errors cancel other than the contribution due to an extra slow π or γ in, for example, $B \to D_s^{*+}\bar{D}/B \to D_s^+\bar{D}$, and the addition of the uncertainty in the D^+ branching fraction scale in $\mathcal{B}(B \to D_s^{(*)+}\bar{D})$. The data favor the prediction that $f_{D_s} = f_{D_s^*}$. The predictions for the ratios of widths using the pole form for the form factors are excluded by the experimental result for $\mathcal{B}(B \to D_s^+\bar{D})/\mathcal{B}(B \to D_s^+\bar{D}^*)$, while the predictions using HQET motivated form factors describe the data well. This is one of the few comparisons of theory with the data that is insensitive to the large uncertainty in $\mathcal{B}(D_s^+ \to \phi\pi^+)$.

VII. FIT TO THE INCLUSIVE D_S^+ MOMENTUM SPECTRUM

Since the B mesons are produced nearly at rest, the two-body decays result in $D_s^{(*)+}$ momentum spectra which are flat distributions, about 300 MeV wide, around the decay momentum. The D_s^{*+} decays predominantly to $D_s^+\gamma$ while the P-wave $c\bar{s}$ mesons, the $D_{s1}^+(2536)$ and $D_{s2}^{*+}(2573)$ [28], decay only to $D^{(*)}K$. Therefore, $B \to D_s^{*+}X$ decays contribute to the inclusive D_s^+ momentum spectrum with distributions which are slightly broadened and shifted down in momentum from the corresponding $B \to D_s^+X$ decay while the other $c\bar{s}$ resonances do not contribute to the inclusive D_s^+ momentum spectrum.

There are two basic mechanisms giving three-body final states. Events of the type $B \to D_s^{(*)+}\bar{D}^{(*)}X$ are produced via the external spectator diagram of Figure 1 but with the popping of an additional $q\bar{q}$ pair. A D_s^- can be produced in B meson decay when an $s\bar{s}$ is produced and the s quark combines with the anti-charm quark from the decay of the $\bar{b}$ quark. These two three-body mechanisms are referred to as "upper-vertex" and "lower-vertex" three-body decays, respectively. The correlation between the charge of the $D_s^\pm$ with that of the B has not been exploited in the analysis of the inclusive D_s^+ momentum spectrum because the flavor of the B which produced the $D_s^\pm$ is not measured [31].

The function used in the fit to the inclusive D_s^+ momentum spectrum includes contributions from the following sources:

(A) $B \to D_s^{(*)+}\bar{D}^{(*)}$ decays. This is the only contribution where the relative branching fractions of the individual contributing channels are known. The predictions and measurements are given in Table X. It is assumed that $f_{D_s} = f_{D_s^*}$. A fit is done for each of the predictions of Table X and the variation in the result is taken as the systematic error due to model dependence.

(B) $B \to D_s^{(*)+}D^{**}$ decays. Only the narrow P-wave charmed states, the $D_1(2420)$ and $D_2^*(2460)$, are used. The contributions from $B \to D_s^+\bar{D}_1(2420)$, $B \to D_s^{*+}\bar{D}_1(2420)$, $B \to D_s^+\bar{D}_2^*(2460)$, and $B \to D_s^{*+}\bar{D}_2^*(2460)$ are added with equal weight. The broad,

not yet observed, 0^+ and 1^+ states are assumed to be taken into account by the three-body or "non-resonant" part of the function described next.

(C) upper-vertex $B \to D_s^{(*)+}\bar{D}^{(*)}\pi/\rho/\omega$ decays. Both the relative amounts of each particle type in these decays and the shape of the resultant D_s^+ momentum spectrum are unknown. The individual shapes are generated according to phase space alone and are added with equal weight.

(D) lower-vertex decays. As in (C), the shapes are generated according to phase space while the relative branching fractions (e.g., $D_s^- K^+\pi^+$ versus $D_s^{*-} K^{*0}\pi^+$) are arbitrary. Lower-vertex decays are expected to be suppressed and are measured to be small [16,31]. This is the only component of the fitting function which contributes D_s^+ mesons in the $x > 0.41$ region. D_s^+ mesons with $x > 0.41$ can be produced in $b \to u$ transitions, and by annihilation and W-exchange diagrams, but these components known to be small [16,17] and are not included in the fit.

As an example, the result of the fit using the ratios of $B \to D_s^{(*)+}\bar{D}^{(*)}$ widths from [20] is shown in Figure 9.

The ratio of the sum of the four $B \to D_s^{(*)+}\bar{D}^{(*)}$ rates to the total inclusive rate is found to be $(45.7 \pm 1.9 \pm 3.7 \pm 0.6)\%$ where the first error is statistical, the second is the systematic error, and the last error represents the the model uncertainty. ARGUS and CLEO-1.5 measured this ratio to be $(58 \pm 7 \pm 9)\%$ and $(56 \pm 10)\%$, respectively [7,8]. The systematic error is dominated by the uncertainty in the shapes of the spectra included in the fitting function. There is no contribution to the systematic error from either the uncertainty in $\mathcal{B}(D_s^+ \to \phi\pi^+)$ or the uncertainty in the tracking efficiency. The contributions to the systematic error due to uncertainty in the shape of the continuum D_s^+ momentum spectrum and due to the uncertainty in the x dependence of the detection efficiency were found to be negligible.

Several methods were used to estimate the systematic error due to the uncertainty in the

shapes of the spectra used in the fit. The fit was repeated for various combinations of (B), (C), and (D) with (A). The inclusive D_s^+ momentum spectrum cannot be fit with a function consisting only of (A) and (D) or (A) and (B). In all cases, the spectrum due to lower-vertex decays, (D), is found to contribute a negligible amount to the total inclusive rate. The D_s^+ yield in the $0.4 < x < 0.5$ region is consistent with continuum background. The fit was also repeated allowing (C) to have three components characterized by how "hard" the constituent spectra were. If $B \to D_s^+ \bar{D}\pi$ is the dominant decay mode of the twelve modes comprising (C), then the spectrum can be fit requiring little or no contribution from (B). Therefore, it is not possible at present to extract from a fit to the inclusive D_s^+ momentum spectrum a meaningful number for any, or even the sum, of the $B \to D_s^{(*)+} D^{**}$ branching fractions.

Using the result of the fit to the inclusive D_s^+ momentum spectrum for the fraction of the $B \to D_s^{(*)+} \bar{D}^{(*)}$ rates to the inclusive rate and the value for the inclusive branching fraction gives $\sum \mathcal{B}(B \to D_s^{(*)+} \bar{D}^{(*)}) = (5.53 \pm 0.23 \pm 0.56 \pm 0.63)\%$ where the first error is statistical, the second is the systematic error, and the third is the error due to the uncertainty in the $D_s^+ \to \phi\pi^+$ branching fraction. This compares well with the statistically less precise value of $\sum \mathcal{B}(B \to D_s^{(*)+} \bar{D}^{(*)}) = (5.52 \pm 0.57 \pm 1.35 \pm 0.63)\%$ which is derived by summing the average branching fractions given in Table VIII.

VIII. EXTRACTION OF THE D_S^+ DECAY CONSTANT

The factorization hypothesis, equation (3), can be used to extract a value for the D_s^+ decay constant from the measured $B \to D_s^{(*)+} \bar{D}^{(*)}$ branching fractions and experimental information on a_1, V_{cb}, and τ_B. Unfortunately, there are large variations in the theoretical predictions for any particular $B \to D_s^{(*)+} \bar{D}^{(*)}$ branching fraction. The parameter a_1 has been derived from $B \to D^{(*)}\pi$ branching fraction measurements [14] but there are at least some theoretical reasons for expecting a_1 to have different values depending on whether the W^+ fragments to $u\bar{d}$ or $c\bar{s}$ [20,32,33].

Some theoretical and experimental errors cancel in the following ratio:

$$\frac{\Gamma(B \to \bar{D}^* D_s^{(*)+})}{d\Gamma(B \to \bar{D}^* e^+ \nu_e)/dq^2|_{q^2=m^2_{D_s^{(*)}}}} = 6\pi^2 (a_1^{c\bar{s}})^2 \delta^{(*)} f^2_{D_s^{(*)}} |V_{cs}|^2 \qquad (4)$$

where $\delta = 0.39$ and $\delta^* = 1.0$ for $B \to D_s^+ \bar{D}^*$ and $B \to D_s^{*+} \bar{D}^*$ decays, respectively[4].

It was found in [18] that

$$\frac{d\Gamma(B \to \bar{D}^* e^+ \nu_e)}{dq^2}|_{q^2=m^2_{D_s}} = 3.17 \pm 0.16 \pm 0.13 \pm 0.14 \pm 0.34 \; ns^{-1}\mathrm{GeV}^{-2}$$

and

$$\frac{d\Gamma(B \to \bar{D}^* e^+ \nu_e)}{dq^2}|_{q^2=m^2_{D_s^*}} = 3.33 \pm 0.16 \pm 0.14 \pm 0.15 \pm 0.34 \; ns^{-1}\mathrm{GeV}^{-2}$$

where the first error is statistical, the second is the error due to the uncertainty in the D and D^* branching fractions, the third is due to the uncertainty in $\tau(B^+)/\tau(B^0)$, and the last is the systematic error associated with detection efficiencies.

Using the average branching fractions, the decay constants are found to be:

$$a_1 f_{D_s} = 319 \pm 31 \pm 32 \pm 18 \text{ MeV}$$

$$a_1 f_{D_s^*} = 286 \pm 28 \pm 26 \pm 16 \text{ MeV}$$

where the first error is statistical and the second is the systematic error which includes the uncertainties in the relative D and D_s^+ branching fractions, and the last is the uncertainty in the $\mathcal{B}(D_s^+ \to \phi\pi^+)$. Averaging the two results under the assumption that $f_{D_s} = f_{D_s^*}$ gives

$$a_1 f_{D_s} = 300 \pm 21 \pm 30 \pm 17 \text{ MeV}.$$

A value for f_{D_s} requiring a ratio of the form factors can be obtained using ratios of hadronic rates like:

---

[4]The analysis in [35] did not include any QCD corrections (i.e., a_1). The kinematic factor δ is calculated to be 0.41 in [35] and 0.39 in [20]. It is shown in [20] that $\delta \to 0.37$ in the limit of infinitely heavy quarks.

$$\frac{\Gamma(B \to \bar{D} D_s^+)}{\Gamma(B^0 \to D^- \pi^+)} = K R_{a_1}^2 \frac{f_{D_s}^2}{f_\pi^2} \frac{|V_{cs}|^2}{|V_{ud}|^2} \frac{|\xi(q^2 = m_{D_s}^2)|^2}{|\xi(q^2 = m_\pi^2)|^2} \tag{5}$$

where K is a calculable kinematic factor and $R_{a_1} \equiv a_1^{c\bar{s}}/a_1^{u\bar{d}}$, with the superscript of a_1 refering to the W^+ fragmentation mode[5]. Note that only B^0 decays can be used in the denominator since the corresponding B^+ decay can proceed through both internal and external W^+ emission.

The branching fractions extracted from the fit to the inclusive D_s^+ momentum spectrum, rather than the results from the full reconstruction, are used as this results in smaller statistical and systematic errors. Using them also gives a good measure of the model dependence since the same form factor parameterization is used for the calculations of both the ratios of $B \to D_s^{(*)+} \bar{D}^{(*)}$ widths used in the inclusive fit and equation (4). The systematic error due to form factor parameterization can then be quantified by examining the spread in f_{D_s} results derived using the different models. Since for any particular model it is the sum of the $B \to D_s^{(*)+} \bar{D}^{(*)}$ branching fractions which results from the fit to inclusive D_s^+ momentum spectrum, the ratio $R_{exp} \equiv \sum \mathcal{B}(B \to D_s^{(*)+} \bar{D}^{(*)}) / \sum \mathcal{B}(B^0 \to \pi^+/\rho^+ D^{(*)-})$ is used, where the denominator is calculated using CLEO measurements [14]. This is compared to the theoretical predictions for the same quantity (call it R_{th}) to extract f_{D_s}. It is assumed that $f_{D_s} = f_{D_s^*}$. The $\bar{u}d$ decay constants are $f_\pi = 131.74 \pm 0.15$ MeV and $f_\rho = 205 \pm 10$ MeV [20].

The results of such an analysis are shown in Table XI. Only the R_{exp} values obtained using HQET motivated form factors were included. The average value is

$$R_{a_1} f_{D_s} = 288 \pm 13 \pm 28 \pm 16 \pm 20 \text{ MeV}$$

where the first error is statistical, the second is the systematic error including the uncertainty in the relative charm branching fractions, the third error is due to the uncertainty in $\mathcal{B}(D_s^+ \to$

---

[5]In all of the calculations discussed in this note, R_{a_1} was assumed to equal 1.

$\phi\pi^+$), and the final error reflects the model uncertainty. This last error is conservatively taken to be the largest deviation from the mean between the different model predictions.

These results for f_{D_s} are consistent with the value obtained by CLEO using $D_s^+ \to \mu^+\nu$ decays [34], as shown in Table XII.

IX. CONCLUSIONS

The result for the inclusive $B \to D_s^+ X$ branching fraction is:

$$\mathcal{B}(B \to D_s^+ X) = (12.11 \pm 0.39 \pm 0.88 \pm 1.38)\%$$

where the first error is statistical, the second is the systematic error, and the third is the error due to the uncertainty in the $D_s^+ \to \phi\pi^+$ branching fraction. It is found from the fit to the inclusive D_s^+ momentum spectrum that the sum of the $B \to D_s^{(*)+}\bar{D}^{(*)}$ rates comprises $(45.7 \pm 1.9 \pm 3.7 \pm 0.6)\%$ of the total inclusive rate, where the last error reflects model dependence. Combining these results gives $\sum \mathcal{B}(B \to D_s^{(*)+}\bar{D}^{(*)}) = (5.53 \pm 0.23 \pm 0.23 \pm 0.63)\%$.

The measurements of the $B \to D_s^{(*)+}\bar{D}^{(*)}$ branching fractions are given in Table VI. The averages of the B^0 and B^- branching fractions are:

$$\mathcal{B}(B \to D_s^+ \bar{D}) = (1.10 \pm 0.17 \pm 0.28 \pm 0.13)\%$$

$$\mathcal{B}(B \to D_s^{*+} \bar{D}) = (0.89 \pm 0.21 \pm 0.20 \pm 0.10)\%$$

$$\mathcal{B}(B \to D_s^+ \bar{D}^*) = (1.12 \pm 0.21 \pm 0.26 \pm 0.13)\%$$

$$\mathcal{B}(B \to D_s^{*+} \bar{D}^*) = (2.41 \pm 0.45 \pm 0.51 \pm 0.29)\%$$

where the first error is statistical, the second error is the systematic error due to the uncertainties in the charmed branching fractions (other than the normalizing modes) and the efficiencies, and the last error is due to the uncertainty in the two normalizing branching fractions, $\mathcal{B}(D_s^+ \to \phi\pi^+)$ and $\mathcal{B}(D^0 \to K^-\pi^+)$. This last error is completely dominated

by the 11% uncertainty in the D_s^+ branching fraction scale. Combining these results gives $\sum \mathcal{B}(B \to D_s^{(*)+} \bar{D}^{(*)}) = (5.52 \pm 0.57 \pm 1.35 \pm 0.63)\%$, in good agreement with the inclusive D_s^+ analysis.

The ratios of rates calculated using factorization and HQET motivated form factors compare well with the data and favor $f_{D_s^*} = f_{D_s}$.

Finally, assuming factorization, the D_s^+ decay constant is extracted from the ratio of the hadronic rate to the semileptonic rate. For $a_1 = 1.07 \pm 0.04 \pm 0.06$, f_{D_s} is found to be $281 \pm 22 \pm 32$ MeV where the first error is statistical and the second is the systematic error including the uncertainties in the charm branching fractions. It is found from ratios of hadronic rates that $f_{D_s} = 288 \pm 13 \pm 32 \pm 20$ MeV where the third error is due to the uncertainty in the form factors.

ACKNOWLEDGMENTS

We gratefully acknowledge the effort of the CESR staff in providing us with excellent luminosity and running conditions. J.P.A., J.R.P., and I.P.J.S. thank the NYI program of the NSF, G.E. thanks the Heisenberg Foundation, K.K.G., M.S., H.N.N., T.S., and H.Y. thank the OJI program of DOE, J.R.P thanks the A.P. Sloan Foundation, and A.W. thanks the Alexander von Humboldt Stiftung for support. This work was supported by the National Science Foundation, the U.S. Department of Energy, and the Natural Sciences and Engineering Research Council of Canada.

REFERENCES

[1] I.I. Bigi *et al.*, Phys. Lett. **323B** (1994) 408.

[2] A. F. Falk, M. B. Wise, and I. Dunietz, Phys. Rev. **D51** (1995) 1183.

[3] CLEO Collaboration, R. Balest *et al.*, Phys. Rev. **D52** (1995) 2661.

[4] CLEO Collaboration, Y. Kubota *et al.*, Nucl. Inst. Meth. **A320** (1992) 66.

[5] G. C. Fox and S. Wolfram, Phys. Rev. Lett. **41** (1978) 1581.

[6] Particle Data Group, L. Montanet *et al.*, Phys. Rev. **D50** (1994) S1.

[7] ARGUS Collaboration, H. Albrecht *et al.*, Z. Phys. C - Particles and Fields **54** (1992) 1.

[8] CLEO Collaboration, D. Bortoletto *et al.*, Phys. Rev. Lett. **64** (1990) 2117.

[9] ARGUS Collaboration, H.Albrecht *et al.*, Phys. Lett. **187B** (1987) 425.

[10] CLEO Collaboration, P.Haas *et al.*, Phys. Rev. Lett. **56** (1986) 2781.

[11] CLEO Collaboration, D. S. Akerib *et al.*, Phys. Rev. Lett. **71** (1993) 3070.

[12] CLEO Collaboration, R. Balest *et al.*, Phys. Rev. Lett. **72** (1994) 2328.

[13] CLEO Collaboration, F. Butler *et al.*, Phys. Rev. Lett. **69** (1992) 2041.

[14] CLEO Collaboration, M. S. Alam *et al.*, Phys. Rev. **D50** (1994) 43.

[15] M. J. Modesitt, Ph.D. Thesis, Purdue University 1995 (unpublished).

[16] ARGUS Collaboration, H. Albrecht *et al.*, Z. Phys. C - Particles and Fields **60** (1993) 11.

[17] CLEO Collaboration, J. Alexander *et al.*, Phys. Lett. **B319** (1993) 365.

[18] CLEO Collaboration, B. Barish *et al.*, Phys. Rev. **D51** (1995) 1014.

[19] M. Bauer *et al.*, Z. Phys. C - Particles and Fields **34** (1987) 103.

[20] M. Neubert, V. Rieckert, Q. P. Xu, and B. Stech, in *Heavy Flavours*, edited by A. J. Buras and H. Lindner (World Scientific, Singapore, 1992).

[21] J. Rosner, Phys. Rev. **D42** (1990) 3732.

[22] D. Du and C. Liu, Phys. Rev. **D48** (1993) 3397.

[23] A. Deandrea *et al.*, Phys. Lett. **B318** (1993) 549.

[24] T. Mannel *et al.*, Phys. Lett. **B259** (1991) 359. The value of the form factor in this paper is extracted from CLEO 1.5 $B \to D^* \ell \nu$ measurements [27]. Three Isgur-Wise functions are examined and $\sim 15\%$ differences in the predicted branching fractions are found. The median predictions are given in Table IX. The difference between the value given in this paper and those quoted in Table IX is due to the different f_{D_s} value that was assumed. All three parameterizations of the Isgur-Wise function gave the same ratios of widths.

[25] N. Isgur and M.B. Wise, Phys. Lett. **B232** (1989) 113; *idem* Phys. Lett. **B237** (1990) 527.

[26] T. Mannel, W. Roberts, and Z. Ryzak, Phys. Rev. **D44** (1991) R18.

[27] CLEO Collaboration, D. Bortoletto *et al.*, Phys. Rev. Lett. **63** (1989) 1667.

[28] CLEO Collaboration, Y. Kubota *et al.*, Phys. Rev. Lett. **72** (1994) 1972.

[29] M. Savage and M. Wise, Phys. Rev. **D39** (1989) 3346.

[30] P. Colangelo, F. De Fazio, and G. Nardulli, Phys. Lett. **B303** (1993) 152.

[31] An analysis using high-momentum leptons to tag the flavor of the b quark is presented in: CLEO Collaboration, X. Fu *et al.*, CLEO CONF95-11 and EPS0169, submitted paper to the International Europhysics Conference on High Energy Physics, Brussels, Belgium, 1995.

[32] B. Grinstein, W. Kilian, T. Mannel, and M. Wise, Nucl. Phys **B363** (1991) 19.

[33] Hai-Yang Cheng, Academia Sinica PREPRINT IP-ASTP-11-94.

[34] CLEO Collaboration, D. Gibaut *et al.*, CLEO CONF95-22 and EPS0184, submitted paper to the International Europhysics Conference on High Energy Physics, Brussels, Belgium, 1995.

[35] D. Bortoletto and S. Stone, Phys. Rev. Lett. **65** (1990) 2951.

TABLES

TABLE I. Measurements of $\mathcal{B}(B \to D_s^+ X)$. The first error is statistical and the second is the systematic error. A value of $\mathcal{B}(D_s^+ \to \phi\pi^+) = (3.5 \pm 0.4)\%$ is common to all measurements so the error on this quantity is not included in the systematic errors.

Experiment	$\mathcal{B}(B \to D_s^+ X)$
CLEO II	$(12.11 \pm 0.39 \pm 0.88)$ %
ARGUS(92) [7]	$(8.34 \pm 1.11 \pm 0.89)$ %
CLEO-1.5 [8]	$(8.74 \pm 1.31 \pm 0.86)$ %
ARGUS(87) [9]	(12.1 ± 3.4) %
CLEO-I [10]	(10.9 ± 2.9) %

TABLE II. Systematic Errors for $\mathcal{B}(B \to D_s^+ X)$.

Source	Error(%)
Signal Shape	1.46
Background Shape	0.36
Continuum Subtraction	0.30
x Dependence of the Efficiency	1.97
Bin Width	0.99
ϕ Mass Interval	0.52
Particle Identification Criteria	0.67
R_2	0.72
Track Quality Criteria	0.27
Angular Selection Criteria	1.12
Monte Carlo statistics	0.29
TOTAL for D_s^+ yield	3.14
$BR(\phi \to K^+K^-)$	1.83
Number of $B\overline{B}$	1.80
Tracking Efficiency	6.00
Total Systematic Error	7.24

TABLE III. The $D_s^{(*)+}$ mass intervals and branching fractions.

Decay Mode	Mass or ΔM Interval (GeV)	Branching Fraction
$D_s^{*+} \to D_s^+\gamma$	$0.132 < m_{D_s^{*+}} - m_{D_s^+} < 0.152$	1.0
$D_s^+ \to \phi\pi^+$	$1.9542 < m_{\phi\pi^+} < 1.9822$	0.035 ± 0.004
Decay Mode	Mass Interval (GeV)	$\mathcal{B}/\mathcal{B}(D_s^+ \to \phi\pi^+)$
$D_s^+ \to K^0K^+$	$1.9532 < m_{K_S^0K^+} < 1.9832$	1.01 ± 0.25
$D_s^+ \to K^{*0}K^+$	$1.9530 < m_{K^{*0}K^+} < 1.9835$	0.95 ± 0.10
$D_s^+ \to \phi\rho^+$	$1.9442 < m_{\phi\rho^+} < 1.9922$	1.86 ± 0.48
$D_s^+ \to \eta\pi^+$	$1.9374 < m_{\eta\pi^+} < 1.9990$	0.54 ± 0.11
$D_s^+ \to \eta\rho^+$	$1.9338 < m_{\eta\rho^+} < 2.0036$	2.86 ± 0.54

TABLE IV. The $D^{(*)}$ mass intervals and branching fractions.

Decay Mode	Mass or ΔM Interval (GeV)	Branching Fraction
$D^{*+} \to D^0\pi^+$	$0.1430 < m_{D^{*+}} - m_{D^0} < 0.1480$	0.681 ± 0.010
$D^{*0} \to D^0\pi^0$	$0.1406 < m_{D^{*0}} - m_{D^0} < 0.1446$	0.636 ± 0.023
$D^0 \to K^-\pi^+$	$1.8457 < m_{K^-\pi^+} < 1.8833$	0.0391 ± 0.0008
Decay Mode	Mass Interval (GeV)	$\mathcal{B}/\mathcal{B}(D^0 \to K^-\pi^+)$
$D^0 \to K^-\pi^+\pi^0$	$1.8355 < m_{K^-\pi^+\pi^0} < 1.8935$	3.43 ± 0.24
$D^0 \to K^-\pi^+\pi^-\pi^+$	$1.849 < m_{K^-\pi^+\pi^-\pi^+} < 1.8800$	2.02 ± 0.11
$D^+ \to K^-\pi^+\pi^+$	$1.8530 < m_{K^-\pi^+\pi^+} < 1.8856$	2.35 ± 0.16

TABLE V. Allowed mass intervals and branching fractions for the non-charmed mesons.

Decay Mode	Mass Interval (GeV)	Branching Fraction
$\pi^0 \to \gamma\gamma$	$0.1200 < m_{\gamma\gamma} < 0.1500$	0.9880 ± 0.0003
$\eta \to \gamma\gamma$	$0.5174 < m_{\gamma\gamma} < 0.5774$	0.388 ± 0.005
$K^0 \to K^0_S \to \pi^+\pi^-$	$0.4877 < m_{\pi^+\pi^-} < 0.5077$	0.3431 ± 0.0014
$\phi \to K^+K^-$	$1.0095 < m_{K^+K^-} < 1.0295$	0.491 ± 0.009
$K^{*0} \to K^+\pi^-$	$0.8461 < m_{K^+\pi^-} < 0.9461$	0.667
$\rho^+ \to \pi^+\pi^0$	$0.6161 < m_{\pi^+\pi^0} < 0.9201$	1.0

TABLE VI. The B meson candidate angular selection criteria.

Decay Mode	$\lvert\cos\theta_B\rvert$	$\lvert\cos\theta_S\rvert$	$\lvert\cos\theta_H\rvert$
$B^+ \to D_s^+ \bar{D}^0$	≤ 0.75	≤ 0.95	-
$B^+ \to D_s^{*+} \bar{D}^0$	≤ 0.75	≤ 0.95	≤ 0.80
$B^+ \to D_s^+ \bar{D}^{*0}$	≤ 0.75	≤ 0.95	≥ 0.35
$B^+ \to D_s^{*+} \bar{D}^{*0}$	≤ 0.85	≤ 0.95	-
$B^0 \to D_s^+ D^-$	≤ 0.75	≤ 0.95	-
$B^0 \to D_s^{*+} D^-$	≤ 0.85	≤ 0.95	≤ 0.80
$B^0 \to D_s^+ D^{*-}$	≤ 0.85	-	≥ 0.35
$B^0 \to D_s^{*+} D^{*-}$	-	-	-

TABLE VII. The efficiency times charmed and non-charmed branching fractions ($\varepsilon \cdot \mathcal{B}$), the number of reconstructed events, and the measured branching fractions for each of the eight B decay channels. The quoted error on $\varepsilon \cdot \mathcal{B}$ is just that due to Monte Carlo statistics. The error on the number of events is purely statistical. The third error in the branching fractions after the statistical and systematic error is the 11% uncertainty in $\mathcal{B}(D_s^+ \to \phi\pi^+)$ which is common to all measurements.

Decay Channel	$\varepsilon \cdot \mathcal{B}$ (10^{-3})	# Events	Branching Fraction (%)
$B^+ \to D_s^+ \bar{D}^0$	2.041 ± 0.008	58.4 ± 10.0	$1.26 \pm 0.22 \pm 0.25 \pm 0.15$
$B^+ \to D_s^{*+} \bar{D}^0$	0.826 ± 0.03	16.1 ± 5.0	$0.87 \pm 0.27 \pm 0.17 \pm 0.10$
$B^+ \to D_s^+ \bar{D}^{*0}$	0.425 ± 0.002	13.5 ± 4.1	$1.40 \pm 0.43 \pm 0.35 \pm 0.17$
$B^+ \to D_s^{*+} D^{*0}$	0.211 ± 0.001	14.9 ± 4.2	$3.10 \pm 0.88 \pm 0.65 \pm 0.37$
$B^0 \to D_s^+ D^-$	1.031 ± 0.007	19.7 ± 5.5	$0.87 \pm 0.24 \pm 0.20 \pm 0.10$
$B^0 \to D_s^{*+} D^-$	0.470 ± 0.003	10.3 ± 3.6	$1.00 \pm 0.35 \pm 0.22 \pm 0.11$
$B^0 \to D_s^+ D^{*-}$	0.868 ± 0.003	18.4 ± 4.5	$0.93 \pm 0.23 \pm 0.16 \pm 0.11$
$B^0 \to D_s^{*+} D^{*-}$	0.384 ± 0.002	17.7 ± 4.4	$2.03 \pm 0.50 \pm 0.36 \pm 0.24$

TABLE VIII. The ratio of charged and neutral decay rates and the average $B \to D_s^{(*)+} \bar{D}^{(*)}$ branching fractions. Equal charged and neutral B meson production rates are assumed.

Decay Mode	$(\mathcal{B}^0/\mathcal{B}^+)(\tau_{B^+}/\tau_{B^0}) = \Gamma^0/\Gamma^+$	Average Branching Fraction (%)
$B \to D_s^+ \bar{D}$	$0.68 \pm 0.22 \pm 0.10$	$1.10 \pm 0.17 \pm 0.28 \pm 0.13$
$B \to D_s^{*+} \bar{D}$	$1.13 \pm 0.53 \pm 0.18$	$0.89 \pm 0.21 \pm 0.20 \pm 0.10$
$B \to D_s^+ \bar{D}^*$	$0.65 \pm 0.25 \pm 0.09$	$1.12 \pm 0.21 \pm 0.26 \pm 0.13$
$B \to D_s^{*+} \bar{D}^*$	$0.65 \pm 0.25 \pm 0.09$	$2.41 \pm 0.45 \pm 0.51 \pm 0.29$

TABLE IX. Predictions for the $B \to D_s^{(*)+}\bar{D}^{(*)}$ branching fractions assuming $|V_{cs}| = 0.974$, $f_{D_s} = f_{D_s^*} = 280$ MeV, $V_{cb} = .038$, $\tau_B = 1.52\ ps$, and $|a_1| = 1.07$ [14], which was derived from $B^0 \to D^{(*)+}\pi^-/\rho^-$ decays. The CLEO II values are the values of Table VIII with all of the errors added in quadrature.

Model	$D_s^+\bar{D}$	$D_s^{*+}\bar{D}$	$D_s^+\bar{D}^*$	$D_s^{*+}\bar{D}^*$
BSW [19]	1.69	0.99	0.76	2.74
Neubert *et al.* [20]	1.25	1.07	1.03	2.76
Du & Liu [22]	1.70	1.14	1.26	3.10
Deandrea *et al.* [23]	1.21	0.83	0.85	3.17
Mannel [24]	0.88	0.56	0.56	1.70
CLEO II	1.10 ± 0.35	0.89 ± 0.31	1.12 ± 0.36	2.41 ± 0.74

TABLE X. Predictions for ratios of widths in $B \to D_s^{(*)+}D^{(*)}$ decays.

Model	$\frac{\Gamma(B\to D_s^{*+}D)}{\Gamma(B\to D_s^{+}D^*)}$	$\frac{\Gamma(B\to D_s^{+}D)}{\Gamma(B\to D_s^{+}D^*)}$	$\frac{\Gamma(B\to D_s^{*+}D^*)}{\Gamma(B\to D_s^{*+}D)}$
BSW [19]	$1.31\,(f_{D_s^*}/f_{D_s})^2$	2.24	2.77
Rosner [21]	$1.00\,(f_{D_s^*}/f_{D_s})^2$	1.43	2.59
Neubert *et al.* [20]	$1.04\,(f_{D_s^*}/f_{D_s})^2$	1.47	2.56
Du & Liu [22]	$0.91\,(f_{D_s^*}/f_{D_s})^2$	1.35	2.72
Deandrea *et al.* [23]	$0.97\,(f_{D_s^*}/f_{D_s})^2$	1.42	3.84
Mannel *et al.* [24]	$1.00\,(f_{D_s^*}/f_{D_s})^2$	1.56	3.01
CLEO II	0.80 ± 0.24	0.99 ± 0.24	2.70 ± 0.81

TABLE XI. The experimental and theoretical values for R, which is defined as $\sum\Gamma(B \to D_s^{(*)+}\bar{D}^{(*)})/\sum\Gamma(B^0 \to \pi^+/\rho^+ D^{(*)-})$, and the resulting f_{D_s} values.

Model	R_{th} (GeV^2)	R_{exp}	f_{D_s} (MeV)
Neubert *et al.*	$35.33 f_{D_s}^2$	2.68 ± 0.23	$275 \pm 12 \pm 25$
Du & Liu	$28.12 f_{D_s}^2$	2.67 ± 0.23	$308 \pm 13 \pm 28$
Deandrea *et al.*	$37.49 f_{D_s}^2$	2.80 ± 0.24	$273 \pm 12 \pm 22$
Mannel	$30.81 f_{D_s}^2$	2.72 ± 0.23	$297 \pm 13 \pm 23$

TABLE XII. Determinations of f_{D_s}. The first error is statistical while the second is the systematic error. A $D_s^+ \to \phi\pi^+$ branching fraction of $(3.5 \pm 0.4)\%$ is common to all results and the uncertainty in $\mathcal{B}(D_s^+ \to \phi\pi^+)$ is not included in the systematic error. Factorization and $f_{D_s} = f_D$; are assumed in the derivations of the values in this paper, given in rows 2 and 3. An a_1 value of $1.07 \pm .04 \pm .06$ [14] was used to get f_{D_s} from the ratio of the hadronic to semileptonic widths. For the f_{D_s} value obtained from the ratios of hadronic widths, it is again assumed that a_1 is independent of whether the W^+ fragments to $\bar{u}d$ or $\bar{c}s$.

Technique	f_{D_s} (MeV)
$D_s^+ \to \mu^+\nu_\mu$	$284 \pm 30 \pm 30$
$\Gamma(B \to D_s^{(*)+}\bar{D}^*)/d\Gamma(B \to \bar{D}^* e^+\nu_e)/dq^2\|_{q^2=m^2_{D_s^{(*)}}}$	$281 \pm 22 \pm 32$
$\sum\Gamma(B \to D_s^{(*)+}\bar{D}^{(*)})/\sum\Gamma(B^0 \to \pi^+/\rho^+ D^{(*)-})$	$288 \pm 13 \pm 38$

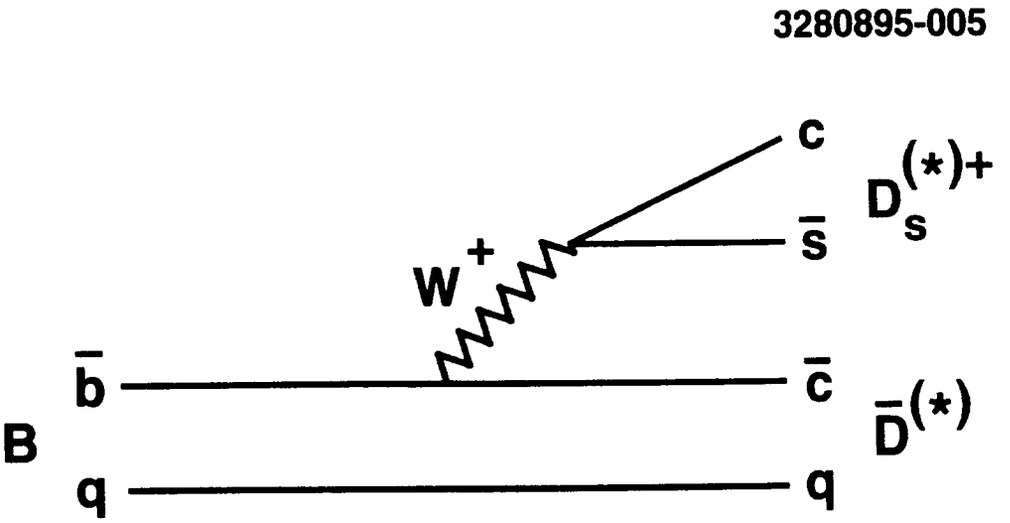

FIG. 1. The spectator diagram for $B \to D_s^{(*)+} \bar{D}^{(*)}$ decay

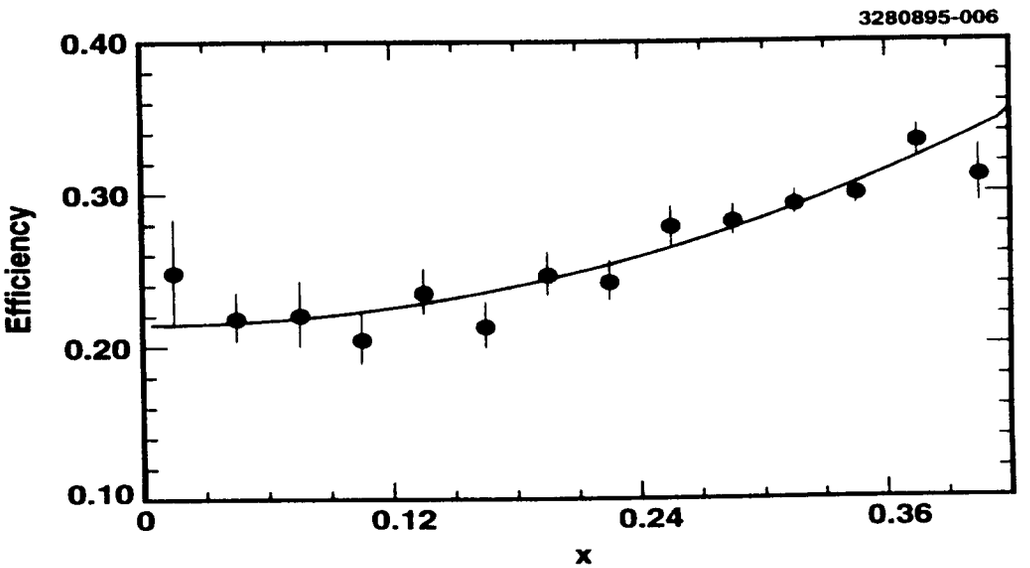

FIG. 2. The efficiency for reconstructing $D_s^+ \to \phi\pi^+, \phi \to K^+K^-$ as a function of scaled D_s^+ momentum for the selection criteria described in the text. The curve is the result of fitting a 2^{nd} order polynomial to the data points.

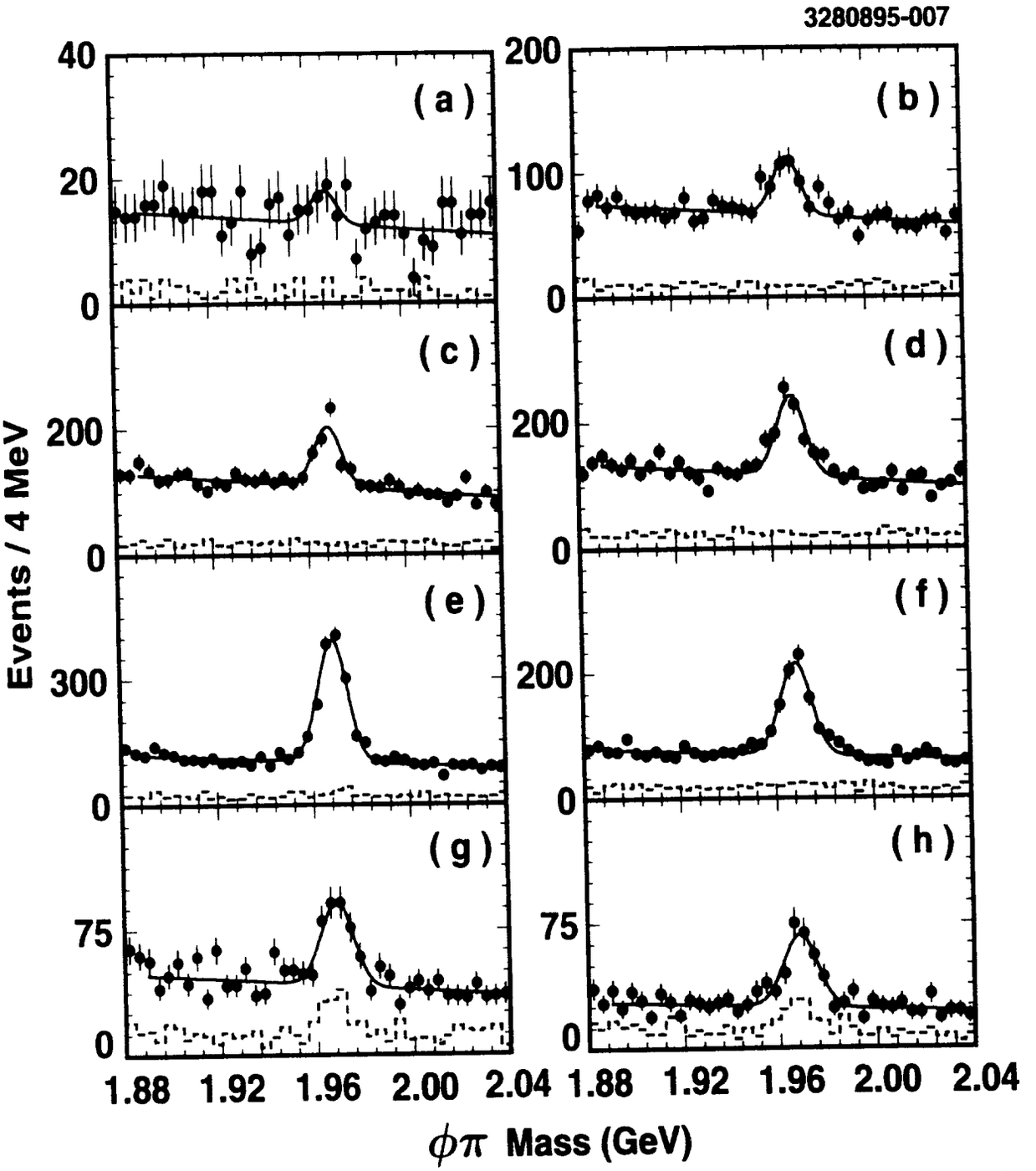

FIG. 3. The $\phi\pi^+$ mass spectra for the on-resonance (points with error bars) and unscaled off-resonance (hatched histogram) data sets in x bins of 0.07 from (a) $0.0 \leq x < 0.07$ to (h) $0.49 \leq x < 0.56$.

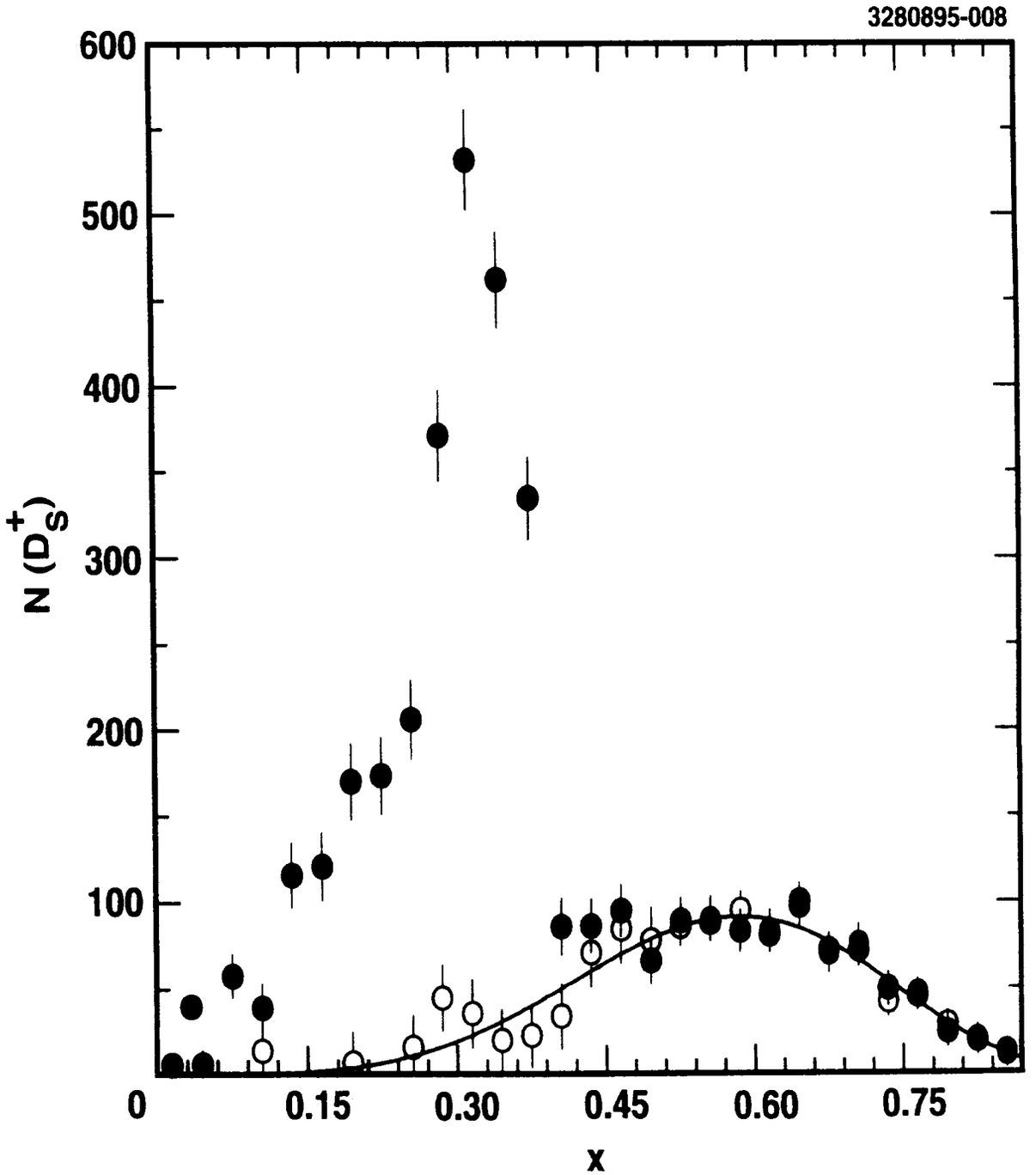

FIG. 4. The on-resonance (solid dots) and scaled 'constructed' continuum (open circles) D_s^+ momentum spectra before efficiency correction. The function is the result of the fit described in the text.

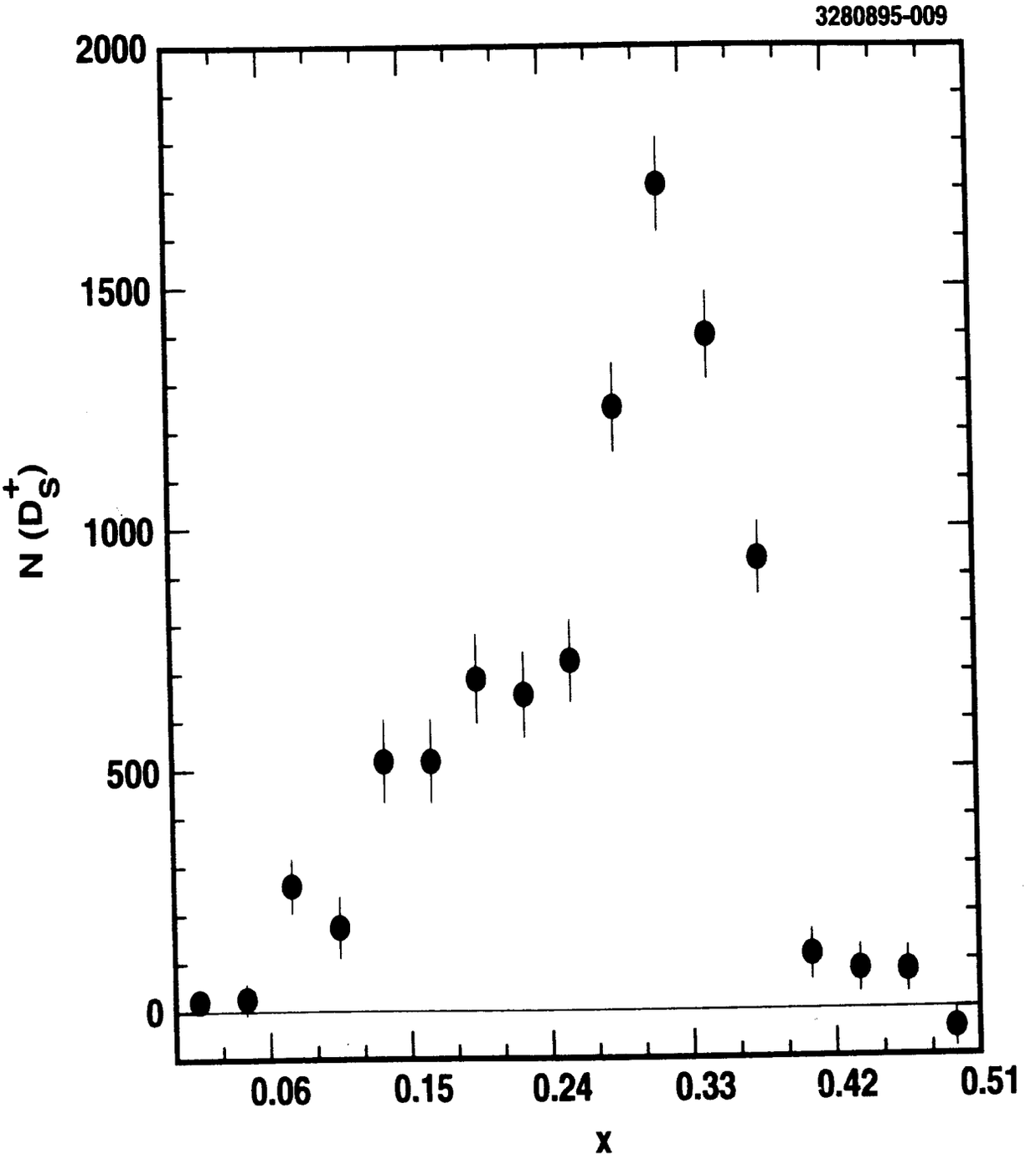

FIG. 5. The continuum-subtracted, efficiency-corrected yield of D_s^+ mesons as a function of x.

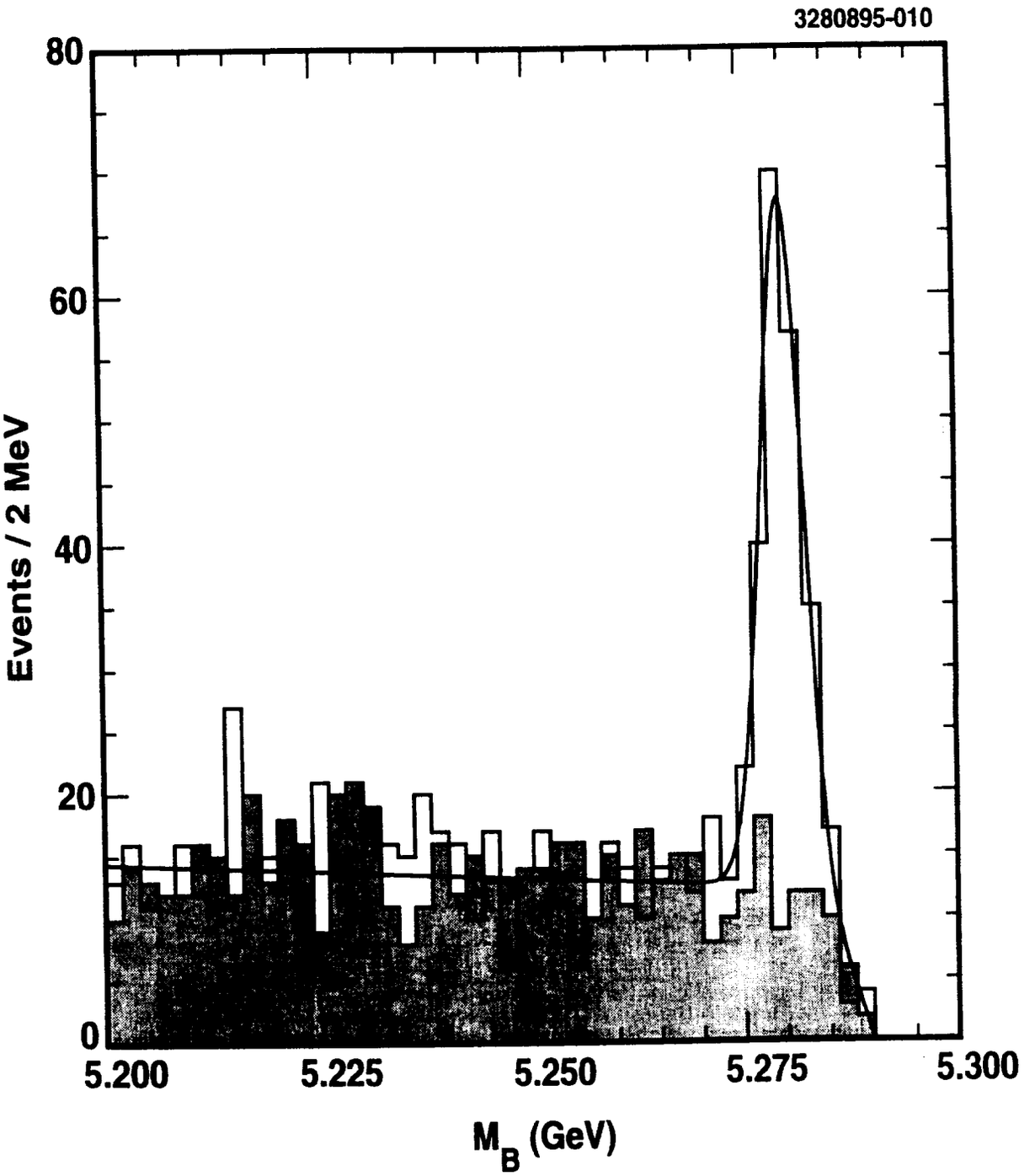

FIG. 6. The beam-constrained mass for the sum of the eight $B \to D_s^{(*)+} D^{(*)}$ modes. The solid histogram is the data within the ΔE signal window while the filled histogram is the data in the ΔE sidebands (as described in the text). The curve is the result of the fit described in the text.

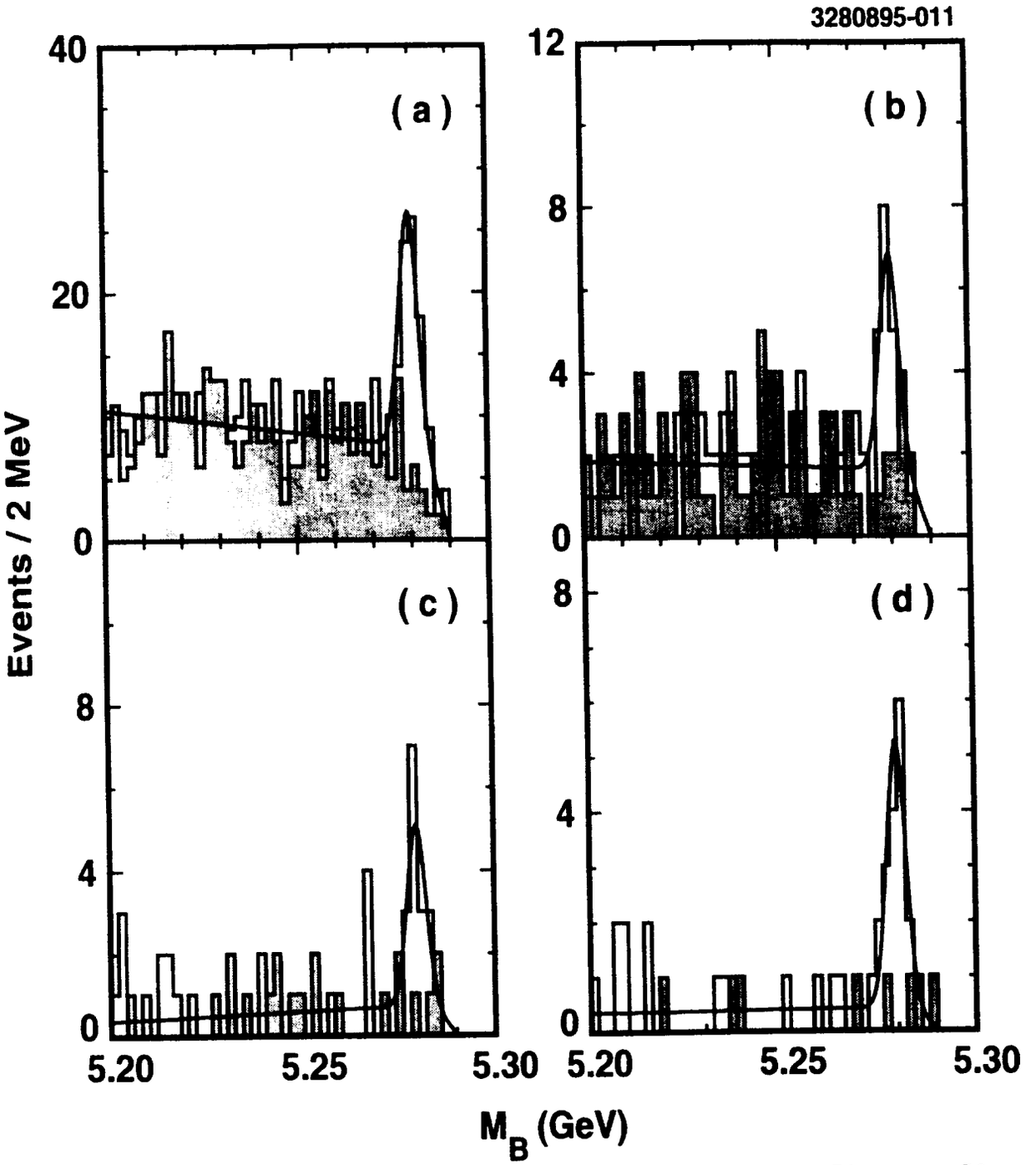

FIG. 7. The beam-constrained mass plots for the B^+ decay modes: (a) $D_s^+\bar{D}^0$, (b) $D_s^{*+}\bar{D}^0$, (c) $D_s^+\bar{D}^{*0}$, and (d) $D_s^{*+}\bar{D}^{*0}$. The solid histogram is the data within the ΔE signal window while the filled histogram is the data in the ΔE sidebands (as described in the text). The curve is the result of the fit described in the text.

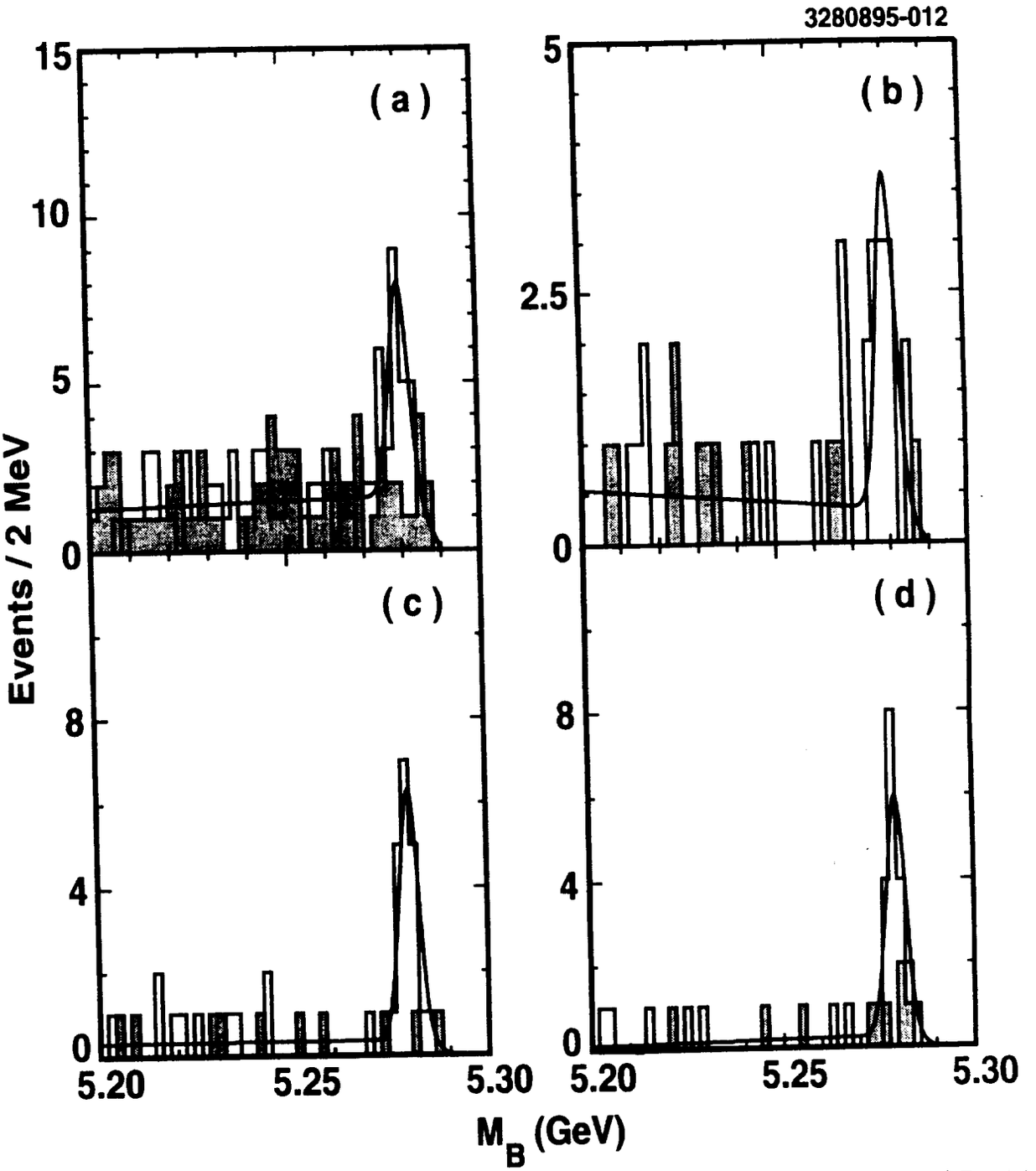

FIG. 8. The beam-constrained mass plots for the B^0 decay modes: (a) $D_s^+ D^-$, (b) $D_s^{*+} D^-$, (c) $D_s^+ D^{*-}$, and (d) $D_s^{*+} D^{*-}$. The solid histogram is the data within the ΔE signal window while the filled histogram is the data in the ΔE sidebands (as described in the text). The curve is the result of the fit described in the text.

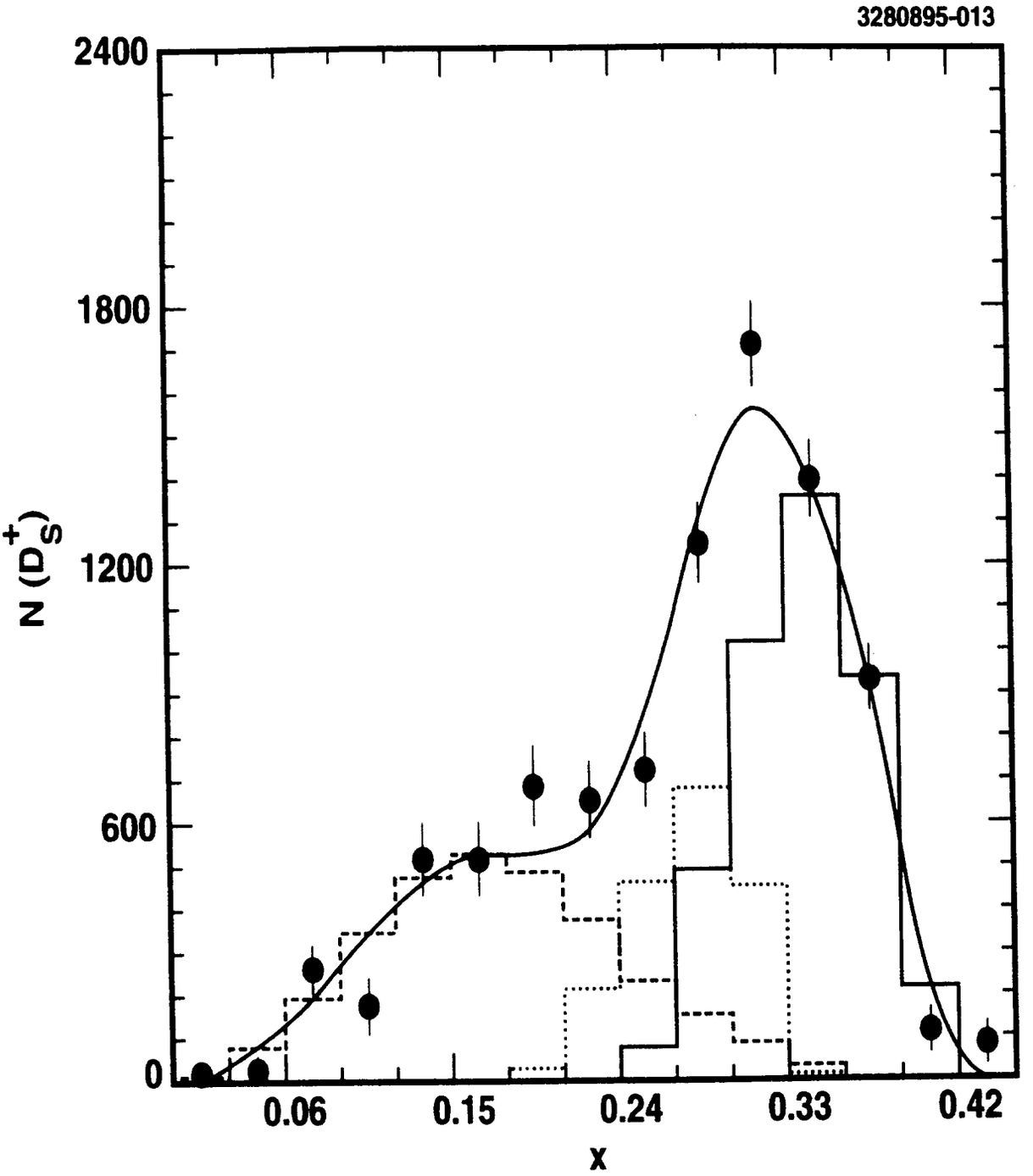

FIG. 9. An example fit to the D_s^+ momentum spectrum. The data are the points with error bars and the smooth curve is the result of the fit. The histograms are the components of the fitting function as described in the text where the solid histogram is (A) – the $D_s^{(*)+}\bar{D}^{(*)}$ component, the dotted histogram is (B) – the $D_s^{(*)+}\bar{D}^{**}$ component, and the dashed histogram is (C) – the $D_s^{(*)+}\bar{D}^{(*)}\pi/\rho$ component.